Heliyon 7 (2021) e06159

Contents lists available at ScienceDirect

Heliyon

journal homepage: www.cell.com/heliyon

Research article

Green synthesis of iron-based nanoparticles using *Chlorophytum comosum* leaf extract: methyl orange dye degradation and antimicrobial properties

Leili Shaker Ardakani [a], Vahid Alimardani [b,*], Ali Mohammad Tamaddon [b,c], Ali Mohammad Amani [d], Saeed Taghizadeh [e]

[a] *Department of Chemistry, Yazd Branch, Islamic Azad University, Yazd, Iran*
[b] *Department of Pharmaceutical Nanotechnology, School of Pharmacy, Shiraz University of Medical Sciences, Shiraz, Iran*
[c] *Center for Nanotechnology in Drug Delivery, Shiraz University of Medical Sciences, Shiraz, Iran*
[d] *Department of Medical Nanotechnology, School of Advanced Medical Sciences and Technologies, Shiraz University of Medical Sciences, Shiraz, Iran*
[e] *Department of Medical Biotechnology, School of Advanced Medical Sciences and Technologies, Shiraz University of Medical Sciences, Shiraz, Iran*

ARTICLE INFO

Keywords:
Green synthesis
Catalytic nanomaterial
Iron nanoparticles
Chlorophytum comosum
Dye degradation
Fenton-like catalyst
Plants extracts

ABSTRACT

Nowadays, green synthesis methods have gained growing attention in nanotechnology owning to their versatile features including high efficiency, cost-effectiveness, and eco-friendliness. Here, the aqueous extract of *Chlorophytum comosum* leaf was applied for the preparation of iron nanoparticles (INPs) to obtain spherical and amorphous INPs with a particle size below 100 nm as confirmed by TEM. The synthesized INPs managed to eliminate methyl orange (MO) from the aqueous solution. The concentration of MO can be easily checked via ultraviolet-visible (UV-Vis) spectroscopy throughout the usage of INPs at the presence of H_2O_2. The synthesized INPs exhibited MO degradation efficiency of 77% after 6 h. Furthermore, the synthesized INPs exhibited antibacterial activity against both Gram-negative and Gram-positive bacteria. The prepared INPs have an impressive effect on *Staphylococcus aureus* at concentrations below 6 μg/ml. Overall, the synthesized INPs could considerably contribute to our combat against organic dyes and bacteria.

1. Introduction

The environmental and industrial applications of nanomaterials have been widely investigated for the detection and degradation of organic contaminants and dyes [1,2,3,4]. Nanoparticles (NPs) can offer more efficient dye degradation owing to their specific physicochemical characteristics such as high surface to volume ratio [5]. So far, a wide variety of NPs including Au [6], CdS [7], TiO_2 [8,9], Manganese-doped ZnO [10], zinc ferrite [11], and iron nanoparticles (INPs) have been successfully used for dye degradation purposes [12]. INPs have been intensively probed for the degradation and removal of organic wastes owing to their versatile properties, high catalytic activities, and highly reactive surface functional groups [13]. Environmental remediation [14], separations and analyses of various analysts [15,16], fungal, parasitic, and bacterial diseases therapies [17,18], drug delivery [19], biosensing [20], imaging [21], catalysis [22], and magnetic storage media [23] can be mentioned as some of the potential applications of NPs.

Lately, INPs were employed as a heterogeneous Fenton-like catalyst for the removal/degradation of numerous organic pollutants in aqueous media [24]. Fenton reagent is a solution of Fe^{2+}/Fe^{3+} and hydrogen peroxide (H_2O_2) which can rapidly oxidize diverse organic contaminants by generating highly reactive hydroxyl radicals ($^{\bullet}OH$) [25]. Among the organic pollutants, azo dyes are of particular concern, as the extensive application of these carcinogenic compounds in different industries has led to their resistance against biological and physicochemical treatments [26,27,28,29,30,31], making the conventional treatment methods ineffective [32]. Various techniques such as hydrothermal [33], sol-gel process [13], chemical co-precipitation [34], template-assisted method [35], thermal decomposition [36], and vapor–solid growth techniques [37] have been exploited for the synthesis of INPs, each suffering from several drawbacks, including a) toxic by-products whose removal requires special treatments, b) high temperature, c) the need for substrate or templates necessitating pre-manufacturing and post-removal difficulties, and d) contaminants which may cause further ecological damages [38,39]. Today, significant efforts have been dedicated to the expansion

* Corresponding author.
E-mail address: v_alimardani@sums.ac.ir (V. Alimardani).

https://doi.org/10.1016/j.heliyon.2021.e06159
Received 10 September 2020; Received in revised form 13 December 2020; Accepted 27 January 2021

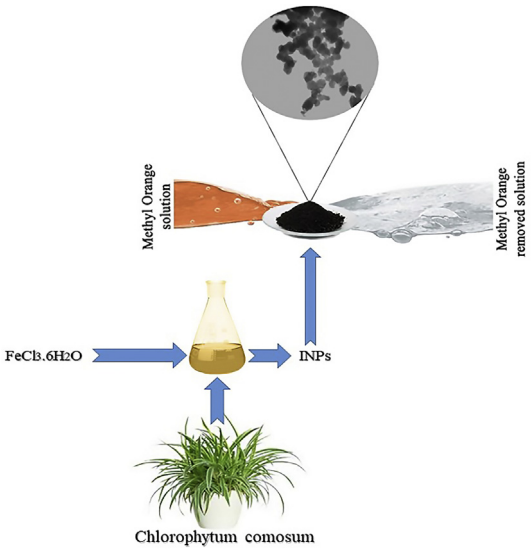

Figure 1. Synthesis of INPs and test its dye degradation performance by decolorization of an azo dye solution.

of green and more environmentally benign processes in the chemical industry.

During the last decades, bacterial and plant-mediated approaches have been developed as a modern synthetic tool to develop green chemical procedures to produce a wide range of INPs in an environmentally-friendly approach [40,41,42,43]. The plant-mediated synthesis of NPs uses non-toxic, biodegradable, and green biomolecules that can act as both reducing and capping agents to minimize the oxidation and agglomeration of the synthesized INPs [44]. For example, *Green tea, Eucalyptus, Tangerine peel, Andean blackberry, Sorghum bran, Argemone Mexicana* extracts have been utilized for the synthesis of different INPs [18,45,46,47,48]. The aqueous leaf extract-mediated production of INPs has been currently studied in the context of *in-vitro* biocompatibility and used for dye removal/degradation [49]. So far, various NPs including metals and carbon-based compounds have been reported for their potential antimicrobial activities [17,50,51,52,53,54]. Hence, in addition to the dye removal/degradation ability of INPs, they have been extensively investigated for their antibacterial properties [55].

The extraordinary features and multifunctional applications of INPs encouraged us to choose the plant extract method for their synthesis. The obtained INPs were then used for the decolorization of an azo dye solution to test their dye degradation performance (Figure 1). In the present study, the applicability of *Chlorophytum comosum* (which is rich in phenol, flavonoid, and saponin contents capable of reducing metal ions and stabilizing the resultant NPs) was explored in the synthesis of INPs [56,57,58]. *Chlorophytum comosum* has been widely assayed for the phytoremediation of pollutants from the indoor air. *Chlorophytum comosum* was also used for the synthesis of INPs as a novel dye removing material [59]. As another application, the antimicrobial activity of the prepared INPs was assessed using the standard microdilution technique.

2. Experimental details

2.1. Chemicals and solvents

Dried *Chlorophytum comosum* leaves were obtained from a local market in Shiraz, Fars, Iran. All chemical reagents including ferric chloride ($FeCl_3{\cdot}6H_2O$), methyl orange (MO, 99.88%), and H_2O_2 solution (30.0%, Merck 64271) were bought from Merck (Darmstadt, Germany) and used without any pretreatment. *Escherichia coli* (ATCC 25922), *Enterococcus faecalis* (ATCC 27852), *Pseudomonas aeruginosa* (ATCC 27852), and *Staphylococcus aureus* (ATCC 25923) were provided from Pasteur Institute of Iran.

2.2. Preparation of leaf extract

Different concentrations of the leaf extract (5–20% w/v) were prepared by mixing dried leaf in deionized water (DI) at 80 °C for 1 h. Next, the extract suspension was cooled to ambient temperature and vacuum-filtered through a 0.2-mm filter paper followed by 5 min of centrifugation (at 2000 rpm) to eliminate the remaining particles. The transparent extract was enclosed in polypropylene tubes and then placed at -20 °C in the refrigerator.

2.3. Synthesis of INPs

The INPs were prepared according to our previous study [60]. Different concentrations of the leaf extract (5%–20% w/v) were used for the synthesis of INPs. Typically, under an inert atmosphere (N_2), 1 ml of

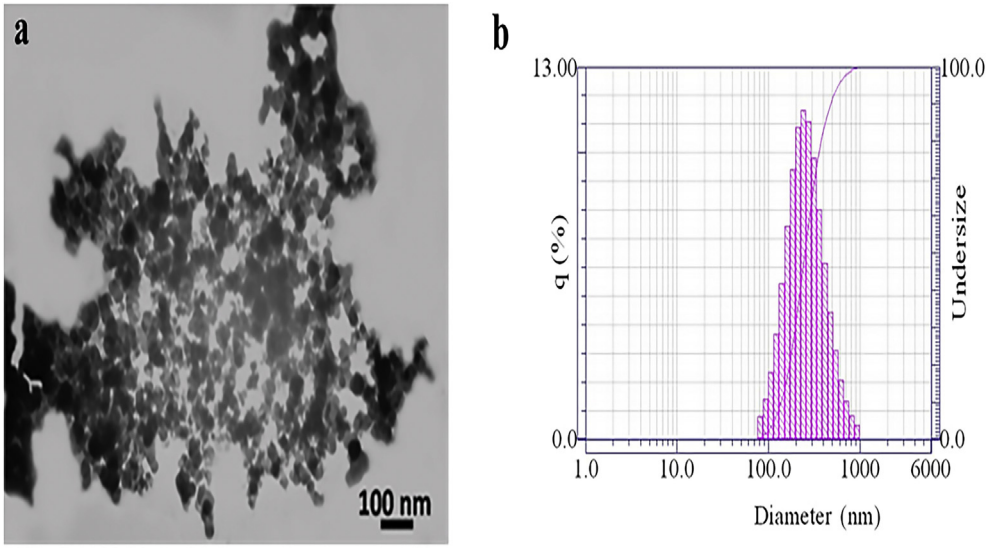

Figure 2. TEM micrographs (a) and PSA histogram (b) of the green synthesized INPs.

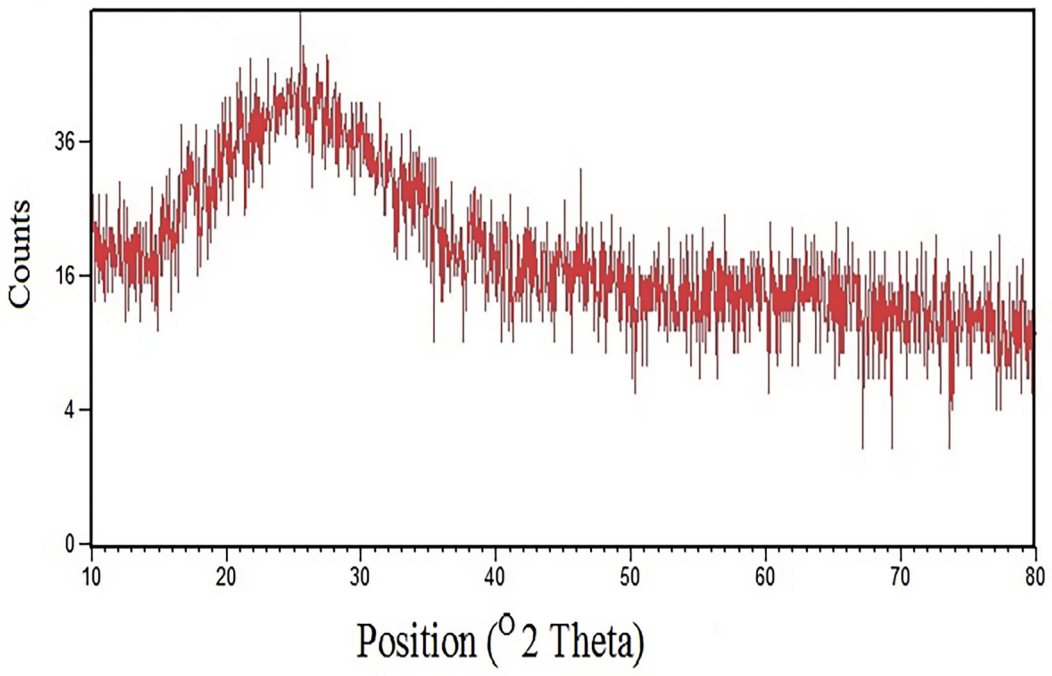

Figure 3. XRD pattern of the green synthesized INPs.

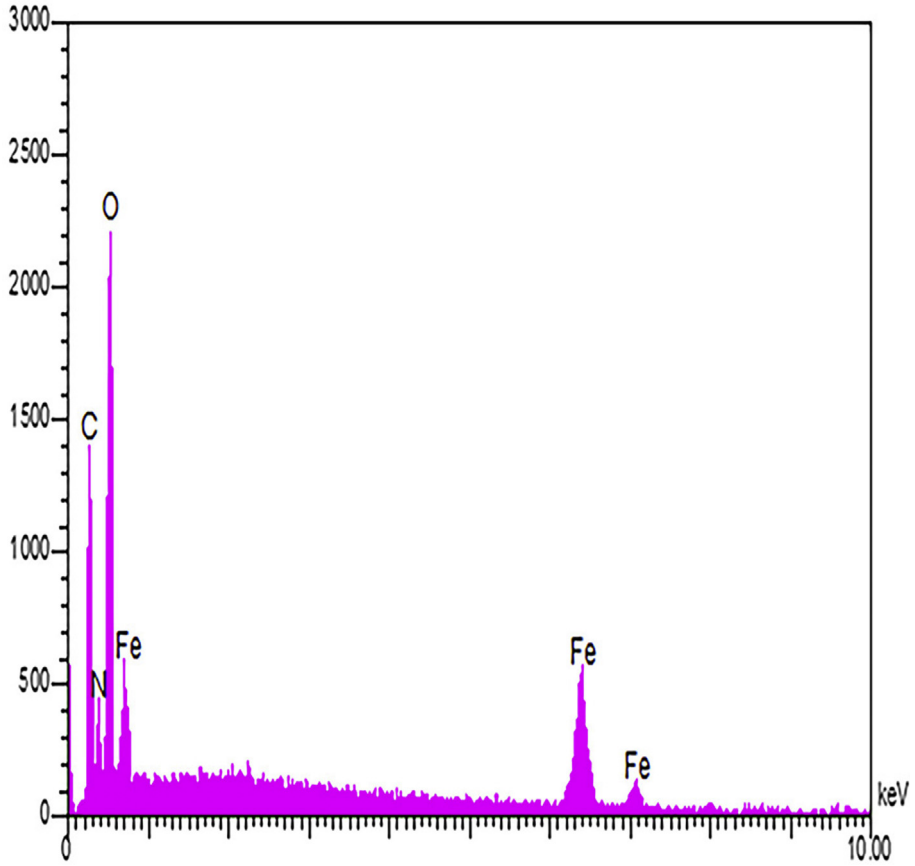

Figure 4. EDX analysis of green synthesized INPs.

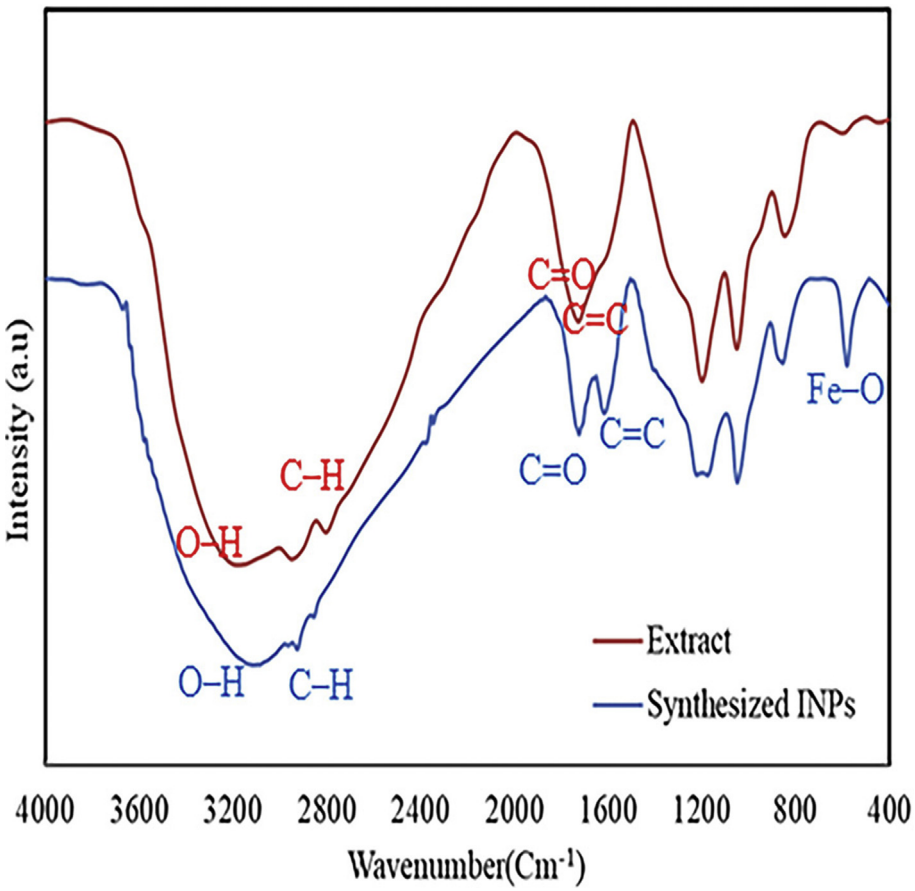

Figure 5. FT-IR spectra of green synthesized INPs.

$FeCl_3 \bullet 6H_2O$, 0.1 M (27 g/L) was added to 9 ml of 5% leaf extract at pH = 6 and poured into a 25-mL round bottom flask and vigorously stirred using a magnetic stirrer (1000 rpm) at ambient temperature for 24 h. Afterward, the reaction media was centrifuged (10,000 rpm for 10 min) to separate the resulting black pellets. Next, the pellets were washed with DI three times, dried in a vacuum oven at 50 °C for 12 h, and stored in a tightly sealed container filled with an inert gas (N_2), in a desiccator for further studies.

2.4. Characterization of INPs

The transmission electron microscopy technique (TEM, Philips CM 10, 100 kV) was used for the morphology and visual appearance analysis of INPs. The particle size was measured by a particle size analyzer (Microtrac S3500). The X-ray powder diffractometry (Siemens D5000, 2Θ range of 10°–80° with 2° min^{-1} scan rate) technique was used for the crystallinity and composition analysis of the INPs. The elemental composition of INPs was evaluated via energy-dispersive X-ray spectroscopy (EDX, BRUKER, INDIA). The FT-IR spectroscopy analyses were performed using a Bruker, Vertex 70, at 4000-400 cm^{-1}. Moreover, the magnetic characteristics of the NPs were evaluated using a vibration sample magnetometer (VSM, Microsense EZ9, at room temperature and field sweeping range of - 10 to + 10 kOe). Finally, the thermogravimetric analysis (TGA, 209 F3 Tarsus, rate of 10 °C/min from 50 °C to 600 °C under Ar atmosphere) was used to assess the presence and quantification of coated organic-compounds on to the surface of INPs.

2.5. Dye removal assay

MO dye was selected to evaluate the dye removal potential of INPs. In a typical procedure, 10 mg of prepared INPs and 1 ml H_2O_2 (10%, optimum concentration) were added to 25-mL flasks containing 8 mL (25 mg l^{-1}) aqueous solution of MO and stirred at 150 rpm at ambient temperature. MO concentrations were measured at different intervals using a UV-Vis spectrophotometer (Hitachi U-0080D, $\lambda_{max} = 465$ nm). The decomposing potential of H_2O_2 was also tested as a blank sample without NPs. All the tests were carried out in triplicate.

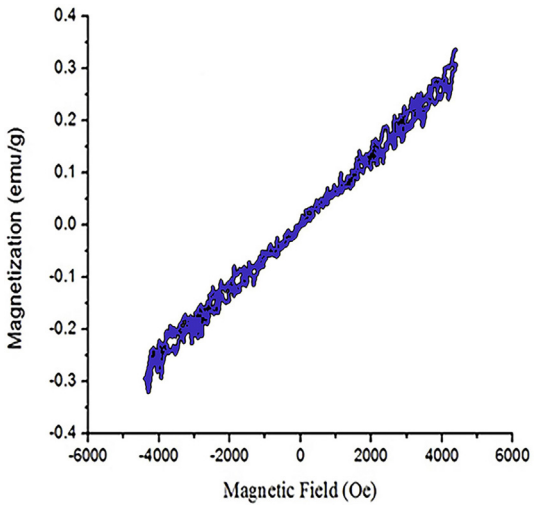

Figure 6. Magnetization curve for the green synthesized INPs.

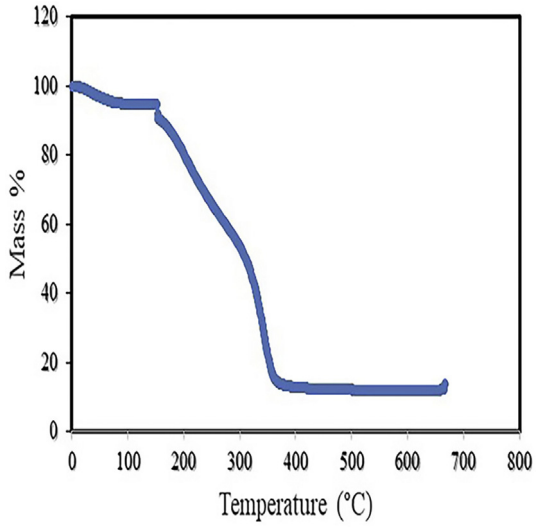

Figure 7. TGA curve of the synthesized INPs.

2.6. Microorganisms and growth conditions

The antimicrobial activity of the prepared INPs was verified via the standard microdilution technique. The results were expressed as the minimum inhibitory concentration (MIC) which can be defined as the lowest concentration of IPNs capable of inhibiting bacterial growth up to 99%. To investigate the antibacterial effect of NPs, several types of Gram-negative (*Escherichia coli* and *Pseudomonas aeruginosa)* and Gram-positive (*Staphylococcus aureus* and *Enterococcus faecalis)* bacteria were utilized [61]. Bacterial culturing was conducted on Mueller– Hinton agar (MHA) at 37 °C for 18–24 h.

3. Results and discussion

Chlorophytum comosum was selected as a model plant for the synthesis of INPs as it showed large reductant contents especially polyphenols compounds. The addition of aqueous *Chlorophytum comosum* leaf extracts to 0.1 M ferric (III) chloride provided an immediate color shift from yellow to dark black implying a notable reduction potential of the leaf extract and the formation of NPs [62]. The main challenges in the production of NPs can be resolved by using micromixing conditions which result in high reaction rates of NPs synthesis and a significant effect on the particle size distribution of NPs. In other words, the quantity of the stirring velocity, and the molar ratio of precursors at the reaction media affected the particle size distribution of NPs [63,64]. The surface morphology and distribution of prepared INPs were investigated by the TEM technique. It can be seen that almost all particles have a spherical shape, smaller than 100 nm with some aggregations (Figure 2a). The hydrodynamic diameter assessment of INPs using PSA displayed that the INPs particle size distribution ranged from approximately 100 to 1000 nm with a mean particle size of 246 nm (Figure 2b). Remarkably, the PSA measured particle size distribution of prepared INPs was different from that measured by the TEM technique due to a biological coating and the connection ability of NPs in aqueous media, resulting in their aggregation. As can be seen in the TEM image, INPs were surrounded by a biological coating produced by the extract which was included in the PSA method. The size distribution of INPs is highly unstable with high aggregation capacity owing to their low surface charge. In other words, the size distribution of INPs changes over time due to their oxidation and the transition in their zeta potential. The oxidation process can lead to an increase in pH resulting in a decline in zeta potential and an aggregation of INPs [65]. So, in chemical synthetic methods, INPs can be stabilized by increasing their surface charge via the addition of citrate ions giving rise to a "citrate coat" around the particles to prevent their interaction (aggregating). On the other hand, the biochemical compounds in the aqueous leaf extract can coat and stabilize INPs and hinder the interactions between NPs, resulting in more stable colloids [66].

X-ray powder diffraction technique demonstrated insufficient distinctive diffraction peaks throughout the pattern reflecting the amorphous nature of the synthesized INPs which is in agreement with reports on using different leaf extracts (Figure 3) [48,66]. A broad peak can be observed at 2θ~ 10°–20° attributable to organic materials from leaf extract which are responsible for capping and stabilizing INPs [48, 62,66].

The EDX analysis indicated the elemental composition of INPs (Figure 4). The EDX analysis showed 25.1% C, 36.75% O, 7.22% N, and 30.93% Fe. In addition to Fe peaks, the emergence of further peaks indicated the existence of organic compounds that were liable for the preparation and stabilization of INPs. FT-IR spectroscopy was also applied to characterize the functional groups of the active components (Figure 5). In the FT-IR spectrum of INPs, the Fe–O stretching band was detected at 516.9 cm^{-1} which was not detected in leaf extract spectra. INPs can react naturally when exposed to air or aqueous media to form a core-shell oxidized INPs [48,67,68]. The peaks at 3200 cm^{-1} in INPs can be assigned to the O–H bond or COOH. The peaks at 2911 and 2863 cm^{-1} are related to the C–H stretching vibration of alkanes of organic compounds of leaf extract. The peak at 1715 cm^{-1} can be also assigned to the C=O stretching vibration of acidic derivatives in the leaf extract. Additionally, the peak at 1635.5 cm^{-1} can be ascribed to the C=C ring stretching indicating the INPs functionalization with organic components [62,69].

The VSM technique was used to study the magnetic properties of the synthesized particles. A linear MH graph with no hysteresis loop was found, showing the paramagnetic behavior of the INPs (Figure 6). Weight loss of the INPs was evaluated in the range of 30–600 °C using TGA (Figure 7). The TGA plot revealed a two-step thermal degradation. Below 200 °C, the mass of INPs fluctuates about 100% related to the elimination of physisorbed water. A sudden weight decline in the next point occurred at 200 °C. Previous works indicated that INPs were decomposed at temperatures up to 200 °C [70].

To determine whether the synthesized INPs can be used for oxidative degradation of MO, the INPs were used as the heterogeneous Fenton-like oxidants for the degradation of MO in an aqueous solution (Figure 8). During the dye removal process, no significant activity was detected for H_2O_2 even after 6h, whereas upon the use of INPs, MO was degraded and the color vanished almost completely with 77% efficiency after 6 h. The spectral band of MO was redshifted from 465 nm to 490 nm after 15 min of incubation with the aqueous mixture of INPs and H_2O_2. This change in the position of the absorption peak might be attributed MO protonation and azonium ions formation [25,71]. MO can be oxidized and decolorized through a Fenton-like reaction in which INPs served as a source of ferrous ions. According to the following formula, a combination of INPs and H_2O_2 can result in the production of free hydroxyl radicals ($OH^{\bullet}$). The azo bond (–N=N–) of MO can decompose by these radicals, resulting in decolorization of the dye contaminated aqueous media [25,72]. The catalytic role of INPs in the Fenton-like process is shown in Figure 9. As can be seen in Figure 8, the INPs efficiently degraded the MO within 6 h. The synthesized IONPs degraded 55% of the initial MO concentration during the first 3 h. Then reduction in color degradation continued at the fourth hour and no significant reduction occurred in the next 2 h. As

Table 1. MIC of synthesized nanoparticles.

Bacteria	MIC (μg/mL)
Staphylococcus aureus	6
Escherichia coli	17
Pseudomonas aeruginosa	9
Enterococcus faecalis	8

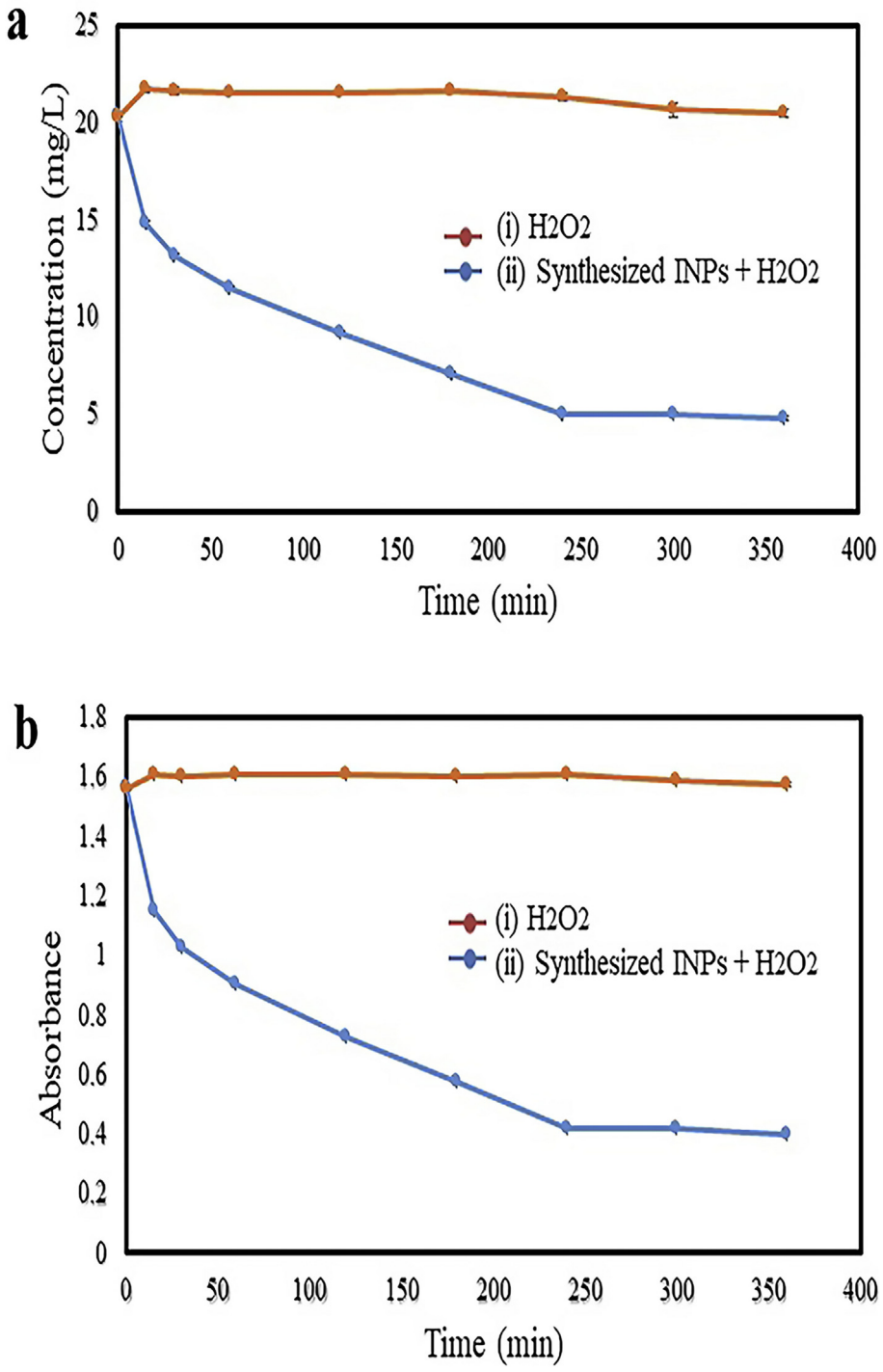

Figure 8. The removal effect of H_2O_2 alone (i) and (ii) H_2O_2 with INPs on the concentration (a) and UV-Vis absorption of MO at different times (b), error bars are too short to display in diagram.

reported by Muthukumar and coworkers, green synthesized INPs have shown better MO degradation than chemically synthesized INPs [73]. Similarly, green synthesized zero valent INPs have also shown significant efficiency in MO degradation; however, noniron NPs such as CuO [74], ZrO_2 [75], and ZnO/SnO_2 nanocomposites [76] demonstrated lower MO degradation efficiency. However, some of the green synthesized NPs like Ag [77] and ZnO [78] demonstrated higher MO degradation efficiency, which can be related to their physicochemical properties like their band gap, size, morphology, and surface coating materials [73]. Overall, green synthesis of INPs can lead to promising results in azo dyes degradation.

The antibacterial effect of biosynthesized INPs was explored on some Gram-positive and Gram-negative bacteria. Table 1 lists the MIC values. Accordingly, the INPs with the lowest concentration dramatically inhibited bacterial growth. This effect was more pronounced on *Staphylococcus aureus* as compared with other bacteria (Table 1) which can be related to their complex cell wall in comparison to the Gram-negative bacteria [79]. Previous reports also suggested higher antimicrobial activity of INPs on Gram-positive bacteria as compared to Gram-negative ones [80]. Several factors can explain the bactericidal mechanisms of metallic oxide NPs. It seems that oxidative stress generated by ROS

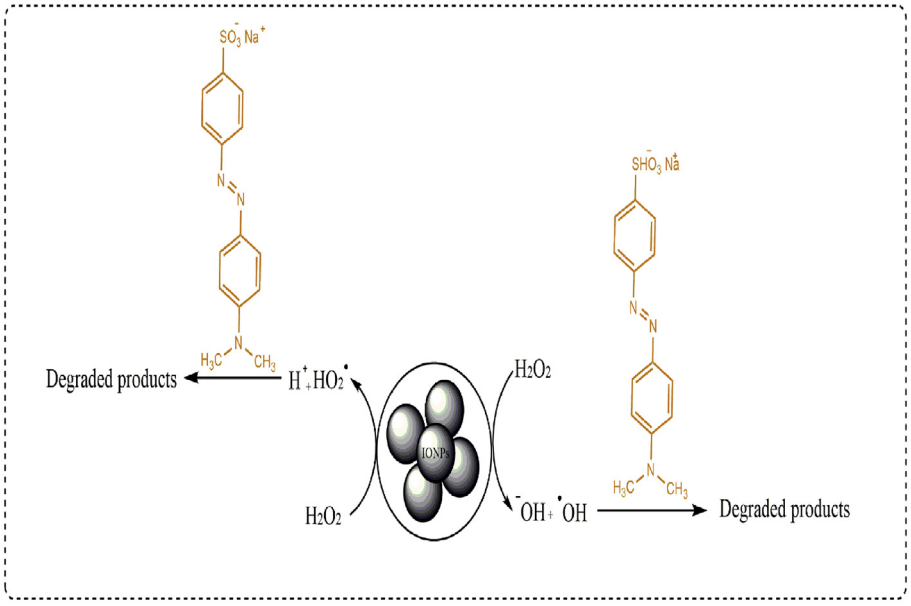

Figure 9. INPs Fenton-like mechanism and MO degradation.

(including superoxide radicals (O_2^-), hydroxyl radicals ($OH^•$), H_2O_2, and singlet oxygen) is the leading player in the antibacterial activity of these NPs. These ROS can damage bacterial proteins and DNA. They can also bind and penetrate the bacterial cell wall, causing structural changes in the cell membrane, such as cell membrane permeability and cell death. A combination of ROS production, gene regulation alternations, cell wall penetration, and metabolite binding simultaneously breaks down the bacterial defense mechanisms against all the interactions [81].

4. Conclusion

In summary, the plant-mediated synthesis of INPs by *Chlorophytum comosum* leaf extract was investigated in this research. The obtained INPs were employed for the MO decolorization and antibacterial purposes. This method uses water dispersion of *Chlorophytum comosum* leaf extract as the only reduction and stabilizing agent added to the iron salt precursor. Thus the present method is an environmentally-friendly method for the preparation of amorphous iron NPs. The dye removal activity of H_2O_2-catalyzed INPs toward the degradation of organic contamination was studied using MO as an azo dye model contaminant. Results showed that the highest efficiency of MO degradation (77%) occurred after 6h. The antibacterial activity of these NPs was investigated on some Gram-negative and Gram-positive bacteria. In accordance with the results, INPs with concentrations below 6 μg/ml has an impressive effect on *Staphylococcus aureus*. Results of antibacterial activity indicated the strong bactericidal effect of these NPs on both Gram-negative and Gram-positive bacteria. Overall, environmentally-friendly INPs can be a valuable candidate for various scientific fields, in particular the removal of organic dyes and the destruction of bacteria.

Declarations

Author contribution statement

Leili Shaker Ardakani: Conceived and designed the experiments; Performed the experiments; Analyzed and interpreted the data.

Vahid Alimardani: Conceived and designed the experiments; Analyzed and interpreted the data; Contributed reagents, materials, analysis tools or data; Wrote the paper.

Ali Mohammad Tamaddon, Ali Mohammad Amani, Saeed Taghizadeh: Conceived and designed the experiments; Analyzed and interpreted the data; Contributed reagents, materials, analysis tools or data.

Funding statement

This research did not receive any specific grant from funding agencies in the public, commercial, or not-for-profit sectors.

Data availability statement

Data included in article/supplementary material/referenced in article.

Declaration of interests statement

The authors declare no conflict of interest.

Additional information

No additional information is available for this paper.

References

[1] K. Simeonidis, S. Mourdikoudis, E. Kaprara, M. Mitrakas, L. Polavarapu, Inorganic engineered nanoparticles in drinking water treatment: a critical review, Environ. Sci.: Water Res. Technol. 2 (2016) 43.
[2] R.L. Singh, P.K. Singh, R.P. Singh, Enzymatic decolorization and degradation of azo dyes – a review, Int. Biodeterior. Biodegrad. 104 (2015) 21.
[3] R.K. Singh, S. Mishra, S. Jena, B. Panigrahi, B. Das, R. Jayabalan, D. Mandal, Rapid colorimetric sensing of gadolinium by EGCG-derived AgNPs: the development of a nanohybrid bioimaging probe, Chem. Commun. 54 (2018) 3981.
[4] R.K. Singh, B. Panigrahi, S. Mishra, B. Das, R. Jayabalan, P.K. Parhi, D. Mandal, pH triggered green synthesized silver nanoparticles toward selective colorimetric detection of kanamycin and hazardous sulfide ions, J. Mol. Liq. 269 (2018) 269.
[5] F. Fu, D.D. Dionysiou, H. Liu, The use of zero-valent iron for groundwater remediation and wastewater treatment: a review, J. Hazard Mater. 267 (2014) 194.
[6] R.K. Singh, S.S. Behera, K.R. Singh, S. Mishra, B. Panigrahi, D. Sahoo Tr andMandal, Biosynthesized gold nanoparticles as photocatalysts for selective degradation of cationic dye and their antimicrobial activity, J. Photochem. Photobiol. Chem. 400 (2020) 112704.
[7] A.S. Bhadwal, R. Tripathi, R.K. Gupta, N. Kumar, R. Singh, A. Shrivastav, Biogenic synthesis and photocatalytic activity of CdS nanoparticles, RSC Adv. 4 (2014) 9484.

[8] N. Lakshmanareddy, V.N. Rao, K.K. Cheralathan, E.P. Subramaniam, M.V. Shankar, Pt/TiO_2 nanotube photocatalyst – effect of synthesis methods on valance state of Pt and its influence on hydrogen production and dye degradation, J. Colloid Interface Sci. 538 (2019) 83.

[9] P. Rath, B. Priyadarshini, S. Behera, P. Parhi, S. Panda, T. Sahoo, Adsorptive removal of Congo Red dye from aqueous solution using TiO_2 nanoparticles: kinetics, thermodynamics and isothermal insights, AIP Conference Proceedings 2115 (2019), 030115.

[10] R. Ullah, J. Dutta, Photocatalytic degradation of organic dyes with manganese-doped ZnO nanoparticles, J. Hazard Mater. 156 (2008) 194.

[11] N.M. Mahmoodi, Zinc ferrite nanoparticle as a magnetic catalyst: Synthesis and dye degradation, Mater. Res. Bull. 48 (2013) 4255.

[12] M.A.J. Kouhbanani, N. Beheshtkhoo, S. Taghizadeh, A.M. Amani, V. Alimardani, One-step green synthesis and characterization of iron oxide nanoparticles using aqueous leaf extract of *Teucrium polium* and their catalytic application in dye degradation, Adv. Nat. Sci. Nanosci. Nanotechnol. 10 (2019), 015007.

[13] M.M. Ba-Abbad, M.S. Takriff, A. Benamor, A.W. Mohammad, Size and shape controlled of α-Fe2O3 nanoparticles prepared via sol–gel technique and their photocatalytic activity, J. Sol. Gel Sci. Technol. 81 (2017) 880.

[14] W-x Zhang, Nanoscale iron particles for environmental remediation: an overview, J. Nano Res. 5 (2003) 323.

[15] M. Shao, F. Ning, J. Zhao, M. Wei, D.G. Evans, X. Duan, Preparation of Fe_3O_4@SiO_2@Layered double hydroxide core–shell microspheres for magnetic separation of proteins, J. Am. Chem. Soc. 134 (2012) 1071.

[16] M. Cao, Z. Li, J. Wang, W. Ge, T. Yue, R. Li, W.Y. William, Food related applications of magnetic iron oxide nanoparticles: enzyme immobilization, protein purification, and food analysis, Trends Food Sci. Technol. 27 (2012) 47.

[17] A. Pugazhendhi, S.S. Kumar, M. Manikandan, M. Saravanan, Photocatalytic properties and antimicrobial efficacy of Fe doped CuO nanoparticles against the pathogenic bacteria and fungi, Microb. Pathog. 122 (2018) 84.

[18] S. Arokiyaraj, M. Saravanan, N.K. Udaya Prakash, M. Valan Arasu, B. Vijayakumar, S. Vincent, Enhanced antibacterial activity of iron oxide magnetic nanoparticles treated with Argemone mexicana L. leaf extract: An in vitro study, Mater. Res. Bull. 48 (2013) 3323.

[19] M. Abedi, S.S. Abolmaali, M. Abedanzadeh, S. Borandeh, S.M. Samani, A.M. Tamaddon, Citric acid functionalized silane coupling versus post-grafting strategy for dual pH and saline responsive delivery of cisplatin by Fe_3O_4/carboxyl functionalized mesoporous SiO_2 hybrid nanoparticles: a-synthesis, physicochemical and biological characterization, Mater. Sci. Eng. C 104 (2019) 109922.

[20] D. Alcantara, S. Lopez, M.L. García-Martin, D. Pozo, Iron oxide nanoparticles as magnetic relaxation switching (MRSw) sensors: current applications in nanomedicine, Nanomed. Nanotechnol. Biol. Med. 12 (2016) 1253.

[21] M. Abedi, S.S. Abolmaali, M. Abedanzadeh, F. Farjadian, S. Mohammadi Samani, A.M. Tamaddon, Core–shell imidazoline–functionalized mesoporous silica superparamagnetic hybrid nanoparticles as a potential theranostic agent for controlled delivery of platinum(II) compound, Int. J. Nanomed. 15 (2020) 2617.

[22] G. Jonathan, Iron/iron oxide nanoparticles: a versatile support for catalytic metals and their application in Suzuki–Miyaura cross-coupling reactions, Chem. Commun. 46 (2010) 2411.

[23] N.A. Frey, S. Peng, K. Cheng, S. Sun, Magnetic nanoparticles: synthesis, functionalization, and applications in bioimaging and magnetic energy storage, Chem. Soc. Rev. 38 (2009) 2532.

[24] X. Wei, X. Xie, Y. Wang, S. Yang, Shape-dependent fenton-like catalytic activity of Fe_3O_4 nanoparticles, J. Environ. Eng. 146 (2020), 04020005.

[25] T. Shahwan, S.A. Sirriah, M. Nairat, E. Boyacı, A.E. Eroğlu, T.B. Scott, K.R. Hallam, Green synthesis of iron nanoparticles and their application as a Fenton-like catalyst for the degradation of aqueous cationic and anionic dyes, Chem. Eng. J. 172 (2011) 258.

[26] Y.-H. Shih, C.-P. Tso, L.-Y. Tung, Rapid degradation of methyl orange with nanoscale zerovalent iron particles, J. Environ. Eng. Manage. 20 (2010) 137.

[27] H. Kusic, N. Koprivanac, L. Srsan, Azo dye degradation using Fenton type processes assisted by UV irradiation: a kinetic study, J. Photochem. Photobiol. Chem. 181 (2006) 195.

[28] C.M.C. da Cruz Brambilla, A.L.H. Garcia, F.R. da Silva, S.R. Taffarel, I. Grivicich, J.N. Picada, S. Knasmüller, Amido Black 10B a widely used azo dye causes DNA damage in pro- and eukaryotic indicator cells, Chemosphere 217 (2019) 430.

[29] K.-T. Chung, C.E. Cerniglia, Mutagenicity of azo dyes: structure-activity relationships, Mutat. Res. Rev. Genet. Toxicol. 277 (1992) 201.

[30] S. Sinha, S. Behera, S. Das, A. Basu, R. Mohapatra, B. Murmu, P. Parhi, Removal of congo red dye from aqueous solution using amberlite IRA-400 in batch and fixed bed reactors, Chem. Eng. Commun. 205 (2018) 432.

[31] S.S. Behera, D. Sourav, P.K. Parhi, S.K. Tripathy, R.K. Mohapatra, D. Mayadhar, Kinetics, thermodynamics and isotherm studies on adsorption of methyl orange from aqueous solution using ion exchange resin amberlite IRA-400, Desalination and Water Treatment 60 (2017) 249.

[32] Z. Zhao, J. Liu, C. Tai, Q. Zhou, J. Hu, G. Jiang, Rapid decolorization of water soluble azo-dyes by nanosized zero-valent iron immobilized on the exchange resin, Sci. China, Ser. B: Chemistry 51 (2008) 186.

[33] S. Ge, X. Shi, K. Sun, C. Li, C. Uher, J.R. Baker Jr., B.G. Orr, Facile hydrothermal synthesis of iron oxide nanoparticles with tunable magnetic properties, J. Phys. Chem. C 113 (2009) 13593.

[34] E. Cheraghipour, A. Tamaddon, S. Javadpour, A. Mehdizadeh, PEGylated superparamagnetic magnetite nanoparticles for magnetic fluid hyperthermia therapy, Res Pharm Sci 7 (2012) 226.

[35] M. Nidhin, R. Indumathy, K. Sreeram, B.U. Nair, Synthesis of iron oxide nanoparticles of narrow size distribution on polysaccharide templates, Bull. Mater. Sci. 31 (2008).

[36] M. Gonzales-Weimuller, M. Zeisberger, K.M. Krishnan, Size-dependant heating rates of iron oxide nanoparticles for magnetic fluid hyperthermia, J. Magn. Magn Mater. 321 (2009) 1947.

[37] D. Maity, D. Agrawal, Synthesis of iron oxide nanoparticles under oxidizing environment and their stabilization in aqueous and non-aqueous media, J. Magn. Magn Mater. 308 (2007) 46.

[38] V.V. Makarov, S.S. Makarova, A.J. Love, O.V. Sinitsyna, A.O. Dudnik, I.V. Yaminsky, N.O. Kalinina, Biosynthesis of stable iron oxide nanoparticles in aqueous extracts of *Hordeum vulgare* and *Rumex acetosa* plants, Langmuir 30 (2014) 5982.

[39] H. Barabadi, K. Damavandi Kamali, F. Jazayeri Shoushtari, B. Tajani, M.A. Mahjoub, A. Alizadeh, M. Saravanan, Emerging theranostic silver and gold nanomaterials to combat prostate cancer: a systematic review, J. Cluster Sci. 30 (2019) 1375.

[40] M. Saravanan, H. Barabadi, B. Ramachandran, G. Venkatraman, K. Ponmurugan, Emerging plant-based anti-cancer green nanomaterials in present scenario. Comprehensive analytical chemistry 87, Elsevier, 2019, p. 291.

[41] H. Barabadi, B. Tajani, M. Moradi, K. Damavandi Kamali, R. Meena, S. Honary, M. Saravanan, Penicillium family as emerging nanofactory for biosynthesis of green nanomaterials: a journey into the world of microorganisms, J. Cluster Sci. 30 (2019) 843.

[42] A. Khatua, E. Priyadarshini, P. Rajamani, A. Patel, J. Kumar, A. Naik, R. Meena, Phytosynthesis, characterization and fungicidal potential of emerging gold nanoparticles using *Pongamia pinnata* leave extract: a novel approach in nanoparticle synthesis, J. Cluster Sci. 31 (2020) 125.

[43] M. Saravanan, V. Jacob, J. Arockiaraj, P. Prakash, Extracellular biosynthesis, characterization and antibacterial activity of silver nanoparticles synthesized by *Bacillus subtilis* (NCIM—2266), J. Bionanoscience 8 (2014) 21.

[44] A. Ebrahiminezhad, A. Zare-Hoseinabadi, A.K. Sarmah, S. Taghizadeh, Y. Ghasemi, A. Berenjian, Plant-mediated synthesis and applications of iron nanoparticles, Mol. Biotechnol. 60 (2018) 154–168.

[45] T. Wang, J. Lin, Z. Chen, M. Megharaj, R. Naidu, Green synthesized iron nanoparticles by green tea and eucalyptus leaves extracts used for removal of nitrate in aqueous solution, J. Clean. Prod. 83 (2014) 413.

[46] M.H. Ehrampoush, M. Miria, M.H. Salmani, A.H. Mahvi, Cadmium removal from aqueous solution by green synthesis iron oxide nanoparticles with tangerine peel extract, J. Environ. Hea. Sci. Engin. 13 (2015) 84.

[47] B. Kumar, K. Smita, L. Cumbal, A. Debut, S. Galeas, V.H. Guerrero, Phytosynthesis and photocatalytic activity of magnetite (Fe_3O_4) nanoparticles using the Andean blackberry leaf, Mater. Chem. Phys. 179 (2016) 310.

[48] E.C. Njagi, H. Huang, L. Stafford, H. Genuino, H.M. Galindo, J.B. Collins, S.L. Suib, Biosynthesis of iron and silver nanoparticles at room temperature using aqueous sorghum bran extracts, Langmuir 27 (2010) 264.

[49] N. Beheshtkhoo, M.A.J. Kouhbanani, A. Savardashtaki, A.M. Amani, S. Taghizadeh, Green synthesis of iron oxide nanoparticles by aqueous leaf extract of *Daphne mezereum* as a novel dye removing material, Appl. Phys. A 124 (2018) 363.

[50] V. Alimardani, S.S. Abolmaali, S. Borandeh, Antifungal and antibacterial properties of graphene-based nanomaterials: a mini-review, J. Nanostruc. 9 (2019) 402.

[51] G. Ren, D. Hu, E.W. Cheng, M.A. Vargas-Reus, P. Reip, R.P. Allaker, Characterisation of copper oxide nanoparticles for antimicrobial applications, Int. J. Antimicrob. Agents 33 (2009) 587.

[52] X. Zhu, K. Pathakoti, H.-M. Hwang, X. Zhu, K. Pathakoti, H.-M. Hwang, Green Synthesis of Titanium Dioxide and Zinc Oxide Nanoparticles and Their Usage for Antimicrobial Applications and Environmental Remediation. Green Synthesis, Characterization and Applications of Nanoparticles, Elsevier, 2019, p. 223.

[53] K. Kanagamani, P. Muthukrishnan, K. Shankar, A. Kathiresan, H. Barabadi, M. Saravanan, Antimicrobial, cytotoxicity and photocatalytic degradation of norfloxacin using *Kleinia grandiflora* mediated silver nanoparticles, J. Cluster Sci. 30 (2019) 1415.

[54] K.C. Hembram, R. Kumar, L. Kandha, P.K. Parhi, C.N. Kundu, B.K. Bindhani, Therapeutic prospective of plant-induced silver nanoparticles: application as antimicrobial and anticancer agent, Artificial cells, nanomedicine, and biotechnology 46 (2018) S38.

[55] M.V. Arasu, S. Arokiyaraj, P. Viayaraghavan, T.S.J. Kumar, V. Duraipandiyan, N.A. Al-Dhabi, K. Kaviyarasu, One step green synthesis of larvicidal, and azo dye degrading antibacterial nanoparticles by response surface methodology, J. Photochem. Photobiol. B Biol. 190 (2019) 154.

[56] S.S. Shinde, S.M. Patil, N.R. Rane, A.A. Adsul, A.R. Gholve, P.K. Pawar, S.P. Govindwar, Comprehensive investigation of free radical quenching potential, total phenol, flavonoid and saponin content, and chemical profiles of twelve Chlorophytum Ker Gawl. species, Indian J. Nat. Prod. Res. (IJNPR)[Formerly Natural Product Radiance (NPR)] 7 (2016) 125.

[57] M.N. Nadagouda, A.B. Castle, R.C. Murdock, S.M. Hussain, R.S. Varma, In vitro biocompatibility of nanoscale zerovalent iron particles (NZVI) synthesized using tea polyphenols, Green Chem. 12 (2010) 114.

[58] G.E. Hoag, J.B. Collins, J.L. Holcomb, J.R. Hoag, M.N. Nadagouda, R.S. Varma, Degradation of bromothymol blue by 'greener' nano-scale zero-valent iron synthesized using tea polyphenols, J. Mater. Chem. 19 (2009) 8671.

[59] H. Gawrońska, B. Bakera, Phytoremediation of particulate matter from indoor air by *Chlorophytum comosum* L. plants, Air Qual. Atmos. Health. 8 (2015) 265.

[60] S. Lohrasbi, M.A.J. Kouhbanani, N. Beheshtkhoo, Y. Ghasemi, A.M. Amani, Taghizadeh, Green synthesis of iron nanoparticles using *Plantago major* leaf extract

and their application as a catalyst for the decolorization of azo Dye, BioNanoScience 9 (2019) 317.
[61] M.A.J. Kouhbanani, N. Beheshtkhoo, P. Nasirmoghadas, S. Yazdanpanah, K. Zomorodianc, S. Taghizadeh, A.M. Amani, Green synthesis of spherical silver nanoparticles using ducrosia anethifolia aqueous extract and its antibacterial activity, J. Environ. Treat. Techn. 7 (2019) 461.
[62] T. Wang, X. Jin, Z. Chen, M. Megharaj, R. Naidu, Green synthesis of Fe nanoparticles using eucalyptus leaf extracts for treatment of eutrophic wastewater, Sci. Total Environ. 466 (2014) 210.
[63] G. Vilardi, N. Verdone, Production of metallic iron nanoparticles in a baffled stirred tank reactor: optimization via computational fluid dynamics simulation, Particuology (2020).
[64] G. Vilardi, M. Stoller, L. Di Palma, K. Boodhoo, N. Verdone, Metallic iron nanoparticles intensified production by spinning disk reactor: optimization and fluid dynamics modelling, Chem. Engin. Process. Proc. Intensification 146 (2019) 107683.
[65] G. Vilardi, M. Parisi, N. Verdone, Simultaneous aggregation and oxidation of nZVI in Rushton equipped agitated vessel: experimental and modelling, Powder Technol. 353 (2019) 238.
[66] Z. Xiao, M. Yuan, B. Yang, Z. Liu, J. Huang, D. Sun, Plant-mediated synthesis of highly active iron nanoparticles for Cr (VI) removal: investigation of the leading biomolecules, Chemosphere 150 (2016) 357.
[67] X-q Li, D.W. Elliott, W-x Zhang, Zero-valent iron nanoparticles for abatement of environmental pollutants: materials and engineering aspects, Crit. Rev. Solid State Mater. Sci. 31 (2006) 111.
[68] K. Sohn, S.W. Kang, S. Ahn, M. Woo, S.-K. Yang, Fe(0) nanoparticles for nitrate reduction: stability, reactivity, and transformation, Environ. Sci. Technol. 40 (2006) 5514.
[69] X. Weng, L. Huang, Z. Chen, M. Megharaj, R. Naidu, Synthesis of iron-based nanoparticles by green tea extract and their degradation of malachite, Ind. Crop. Prod. 51 (2013) 342.
[70] Z. Durmus, H. Kavas, M.S. Toprak, A. Baykal, T.G. Altınçekiç, A. Aslan, S. Coşgun, l-lysine coated iron oxide nanoparticles: Synthesis, structural and conductivity characterization, J. Alloys Compd. 484 (2009) 371.
[71] J. Oakes, P. Gratton, Kinetic investigations of the oxidation of methyl orange and substituted arylazonaphthol dyes by peracids in aqueous solution, J. Chem. Soci. Perkin Transactions 2 (1998) 2563.
[72] Z. Wang, C. Fang, M. Megharaj, Characterization of iron–polyphenol nanoparticles synthesized by three plant extracts and their fenton oxidation of azo dye, ACS Sustain. Chem. Eng. 2 (2014) 1022.
[73] H. Muthukumar, M. Matheswaran, *Amaranthus spinosus* leaf extract mediated FeO nanoparticles: physicochemical traits, photocatalytic and antioxidant activity, ACS Sustain. Chem. Eng. 3 (2015) 3149.
[74] H.S. Devi, T.D. Singh, Synthesis of copper oxide nanoparticles by a novel methodand its application in the degradation of methyl orange, Adv. Electronic Electric Engin. 4 (2014) 83.
[75] T. Sreethawong, S. Ngamsinlapasathian, S. Yoshikawa, Synthesis of crystalline mesoporous-assembled ZrO_2 nanoparticles via a facile surfactant-aided sol–gel process and their photocatalytic dye degradation activity, Chem. Eng. J. 228 (2013) 256.
[76] W. Ali, H. Ullah, A. Zada, M.K. Alamgir, W. Muhammad, M.J. Ahmad, A. Nadhman, Effect of calcination temperature on the photoactivities of ZnO/SnO_2 nanocomposites for the degradation of methyl orange, Mater. Chem. Phys. 213 (2018) 259.
[77] U-e-S Amjad, L. Sherin, M.F. Zafar, M. Mustafa, Comparative study on the catalytic degradation of methyl orange by silver nanoparticles synthesized by solution combustion and green synthesis method, Arabian J. Sci. Eng. 44 (2019) 9851.
[78] V. Gawade, N. Gavade, H. Shinde, S. Babar, A. Kadam, K. Garadkar, Green synthesis of ZnO nanoparticles by using *Calotropis procera* leaves for the photodegradation of methyl orange, J. Mater. Sci. Mater. Electron. 28 (2017) 14033.
[79] L. Wang, C. Hu, L. Shao, The antimicrobial activity of nanoparticles: present situation and prospects for the future, Int. J. Nanomed. 12 (2017) 1227.
[80] Y.-H. Hsueh, P.-H. Tsai, K.-S. Lin, W.-J. Ke, C.-L. Chiang, Antimicrobial effects of zero-valent iron nanoparticles on gram-positive *Bacillus* strains and gram-negative *Escherichia coli* strains, J. Nanobiotechnol. 15 (2017) 77.
[81] Y.N. Slavin, J. Asnis, U. Häfeli Uo, H. Bach, Metal nanoparticles: understanding the mechanisms behind antibacterial activity, J. Nanobiotechnol. 15 (2017) 65.